

Preliminary Study on Hybrid Manufacturing of the Electronic-Mechanical Integrated Systems (EMIS) via the LCD Stereolithography Technology

Guanghai Fei¹, Tiwei Wei², Qimin Shi¹, Yongjian Guo¹, Herman Oprins², Shoufeng Yang^{1,3,*}

¹Department of Mechanical Engineering, Member of Flanders Make, KU Leuven, Leuven 3001, Belgium

²IMEC, Leuven 3001, Belgium

³Materials Research Group, Faculty of Engineering and the Environment, University of Southampton, Southampton SO17 1BJ, UK

Abstract

Compared to limited complexity capacity in traditional fabrication and assembly techniques, Additive Manufacturing (AM)-based hybrid fabrication is emerging in electronics industry for fabricating complex structures and simplifying the assembly steps. In this study, the fabrication process of the Electronic-Mechanical Integrated Systems (EMIS) is investigated, in which mechanical parts (gas/liquid chambers) were 3D printed directly on PCB substrate (the carrier of electronic devices). A mixture of resin with silica was used as printing feedstock, to reduce mismatch of thermal expansion coefficient (CTE) between the part and PCB. The silica loading of 60 vol% was appropriate to achieve a compromise between viscosity of the suspension and CTE. Adhesion forces between printed parts and PCBs were measured, showing a significant correlation with the PCB surface roughness. Thermal cycling test indicated that the tailored materials owned excellent CTE compatibility with PCB. Consequently, AM-based hybrid manufacturing is capable of fabricating protective/functional bodies for electronics.

Keywords: *Hybrid manufacturing, Electronics devices, Stereolithography, Adhesion, Thermal reliability*

Introduction

Fabricating entire systems with both electrical units and mechanical content through on-demand hybrid manufacturing methods has vast potential for high-value electronic devices[1-6]. Among all of the fabrication methods, Additive Manufacturing (AM)-based hybrid manufacturing is emerging in this new paradigm for its advantages. For example, 3D printing fabricates parts with complex shapes and intricate internal microstructures, as well as simplifies the manufacturing process by merging complicated steps of assembly. Besides, because of the powerful manufacturing capabilities, the AM method provides unlimited freedom of design for the engineers, who can focus more on achieving the functionality but less on fabrication.

Recently, this multiprocess 3D printing (or AM-based hybrid manufacturing) is mainly applied in 3D structure electronics[3-8] and 3D packaging engineering [9-14]. The 3D structure electronics can achieve multifunctionality while reducing the part volume, and the 3D package technology is becoming a possible alternative process for the fan-out wafer-level package. Apart from the 3D structure electronics and 3D package technology, the AM-based hybrid manufacturing also has a large market in other microelectronic applications. In this study, we present an Electronic-Mechanical Integrated System (EMIS) manufacturing method; by integrating stereolithography (SLA) and traditional printed circuit board (PCB) manufacturing technique, we can fabricate integrated systems containing both electronic units/devices and mechanical contents.

To describe this EMIS fabrication process more intuitively, we take a Lab-on-a-chip system (LOC) as an example[15]. As shown in Fig. 1, in order to simplify the manufacturing process and to merge complex assembly steps, the AM-based hybrid manufacturing can be used in this case. The Electronic devices (including the USB interface, MCS Module, PCB) can be first made via tradition methods; after that, mechanical parts (for example,

gas generator and other chambers) can be 3D printed directly on the PCB or Cu layer by AM technology. Through this type of EMIS manufacturing method, high power chip cooling systems [16-18] can be fabricated as well.

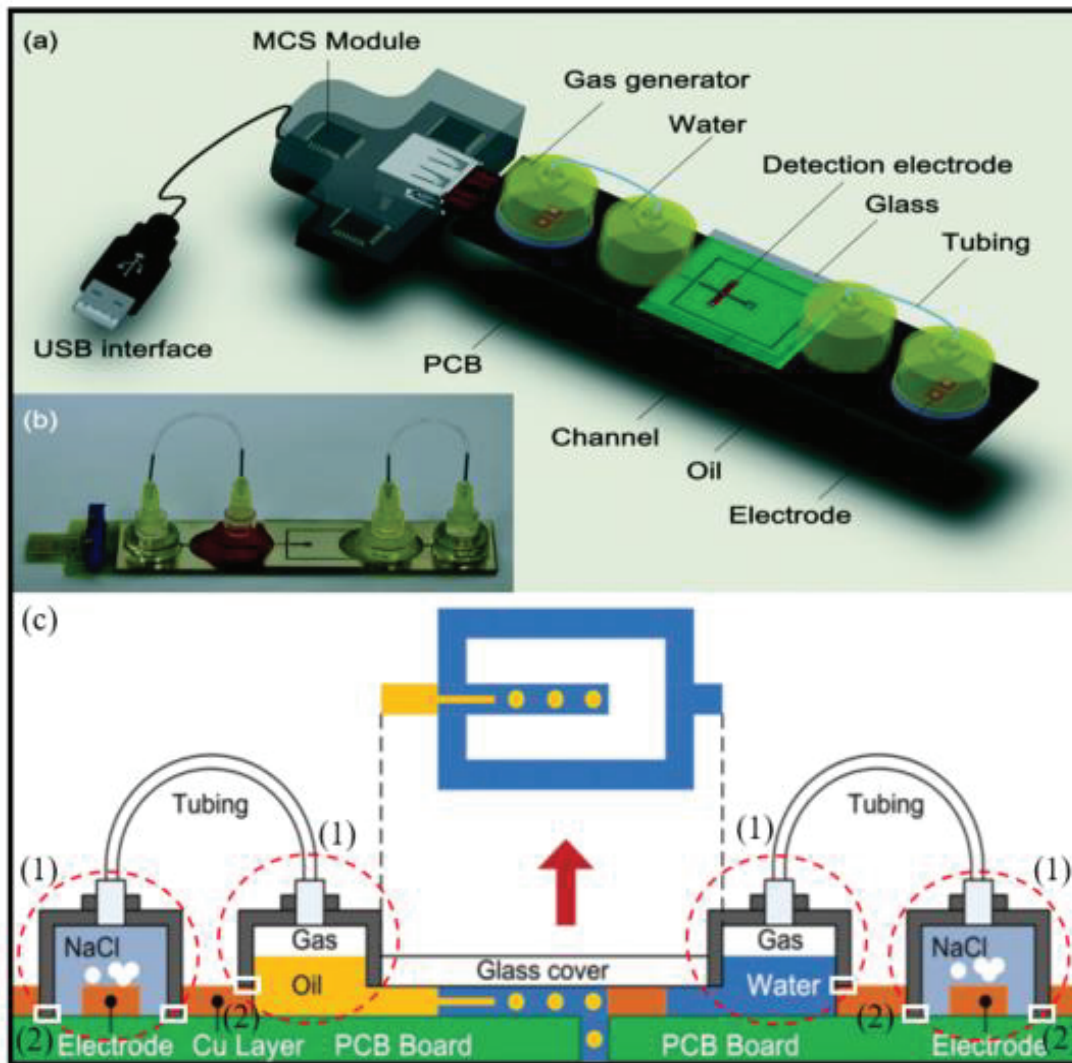


Fig. 1. Schematics of USB-driven microfluidic chips on PCB. (a) 3D schematics of the USB-driven microfluidic device on a PCB (U-Chip), (b) Fabricated U-chip on a PCB with a standard USB interface, (c) Important factors should be taken into account if the parts are directly printed on the PCB; reproduced from [15]

However, no matter the EMIS manufacturing method is used for fabricating *chip cooler* or *LOC*, several essential factors that should be taken into account when the parts are directly printed on the substrate (PCB and wafer) or Cu layer (Fig. 1. (c)). First, an advanced 3D printing technology is needed to print some spans and cavities without supports, because it is hard to remove these supports after printing without the separation of the part from the substrate (Fig. 1. (c)-(1)). Second, to ensure the integrity of the part together with the substrate, a strong bonding force is necessary at the interface between printed parts and substrate (Fig. 1. (c)-(2)). Finally, because of the mismatch in material between the printed parts and substrate, when the whole system was operating, the mismatch of thermal expansion coefficient (CTE) will lead to crack and leakage at the interface. Searching a good CTE compatibility material for the part is a challenge as well.

To solve these issues, we find some solutions both on the AM technology and materials preparation. The bottom-up LCD-based SLA technology was applied to fabricate the cavities (no supports needed). A mixture of resin with silica was applied as the printing feedstock to reduce the mismatch in CTE between the part and the PCB substrate. Adhesion forces and thermal reliability were tested after the printing to evaluate the part-substrate integrity and thermal shock resistance, respectively.

Experimental Details

Material preparation

As mentioned above, to reduce the CTE mismatch between different materials, the photopolymerizable suspension was prepared by adding ceramic powder into a solution of resin. Silica powder, as the most common filler for the microelectronic packaging industry, was selected, due to its optimum combination of properties [19-22]. For example, it exhibits a low CTE (~ 0.55 ppm/ $^{\circ}$ C) and a low enough abrasiveness to provide a relatively long-running lifetime. Besides, fused silica is transparent to UV light, and is therefore appropriate for UV curing. The silica filler used in this study is electronic grade spherical silica powder (Spheroidization rate $\sim 95\%$, SS1402, Industrial Powder, US) with a specific surface area of $\sim 4\text{m}^2/\text{g}$ and a density of $\sim 2.2 \times 10^3\text{kg}/\text{m}^3$. The mean particle size (D50) of the silica powder is $\sim 2\mu\text{m}$. The commercial resin mixture (GP001-JC, Shenzhen Esun Industrial Co., Ltd., China) was a blend of acrylic oligomers (Bisphenol A epoxy diacrylate), monomer (HDDA) and photoinitiator (Irgacure 184). Working together with an alkylammonium salt dispersant (BYK-9076, BYK-Chemie GmbH, Germany), a stable dispersion of the silica in the resin was prepared.

According to the simple rule-of-mixture [23-25], the CTE of a two-phase composite is dependent linearly on the volume fraction of the filler. The most common equation for predicting the CTE of a two-phase composite is expressed as follows:

$$\alpha_c = V_r \cdot \alpha_r + (1 - V_r) \cdot \alpha_s \quad (1)$$

where α_c , α_r and α_s are the CTE of the composite, resin and silica, respectively; V_r is the volume fraction of resin.

From the above equation (1), with the increase of the silica loading, the CTE of composite decreases; while the viscosity of the slurry increase, which makes the slurry too viscous to print. Therefore, we must achieve a compromise between the printability and the CTE. The CTE for the used photosensitive resin and the PCB substrate are ~ 60 ppm/ $^{\circ}$ C (below glass transition temperature) and ~ 20 ppm/ $^{\circ}$ C, respectively. Substituting 0.55 ppm/ $^{\circ}$ C as the CTE of silica, we can initially estimate the volume fraction of silica. Thus, in order to eliminate the mismatch of CTE between the composite and the PCB substrate, ideally, we should achieve 20 ppm/ $^{\circ}$ C for the CTE of composite, in which 32 vol.% of resin and 68 vol.% of silica are needed. However, the viscosity of such resin mixture with 68 vol.% silica is too high. Hence, we adopted a suitable ceramic-resin slurry which consists of 60 vol.% silica powder and 40 vol.% resin mixtures, stabilized to create a fluid suspension using the BYK-9076 dispersant.

In order to achieve a uniform distribution of ceramics within the mixture, silica powder and dispersant were gradually mixed into the resin mixtures; then the suspension was homogenized in a high-speed mixer for 10 min and an ultrasonic cleaner with 30°C for 2 hours.

The LCD-based apparatus and samples manufacturing

Comparing with other AM technologies for polymer-matrix composites, such as fused deposition modeling and inkjet printing, stereolithography system has competitive edges due to its precision, efficiency, low cost, and easy processability [26-28]. A Liquid Crystal Display (LCD) SLA system (isun3d Tech., UV light resin LCD photocurable 3d printer, Shenzhen) was used to print the part at the KU Leuven Additive Manufacturing Lab. As shown in Fig. 2, the LCD-based SLA machine, uses an LCD screen as a photomask—like a filter with many small windows above the Light Emitting Diode (LED) light source. The “windows” on the LCD screen will selectively open/close, to traverse/block off the UV light. The UV light, which passes through the LCD screen, cures the liquid slurry in the tank to form the object. After one layer is finished, the platform is lifted to separate the cured part from the film. The machine solidifies the part layer after layer in this repeating mode. Since LCD screens are inexpensive and can ensure a relatively high printing resolution, this technology has made resin 3D printing much more affordable than before and is becoming more popular than the laser-based SLA and DLP-based SLA.

To fabricate the parts directly on the PCB substrate, first, the PCB should be fixed on the printer platform. A vacuum suction system (shown in Fig. 2) seems to be a good solution to provide a suction strong enough to the PCB during printing. Besides, this system also benefits from easy removing of the PCB from the platform after printing. In addition to manufacturing the 3D parts, some simple samples were fabricated for the CTE test under

the same process parameters. The printing parameters for all samples and 3D parts were as following; UV light wavelength: 405nm, thickness: 0.1mm, bottom layers: 5 layers. The first five layers (denoted ‘bottom layers’) were exposed to the UV light for 45 seconds each, and the other layers were exposed for 8 seconds per layer.

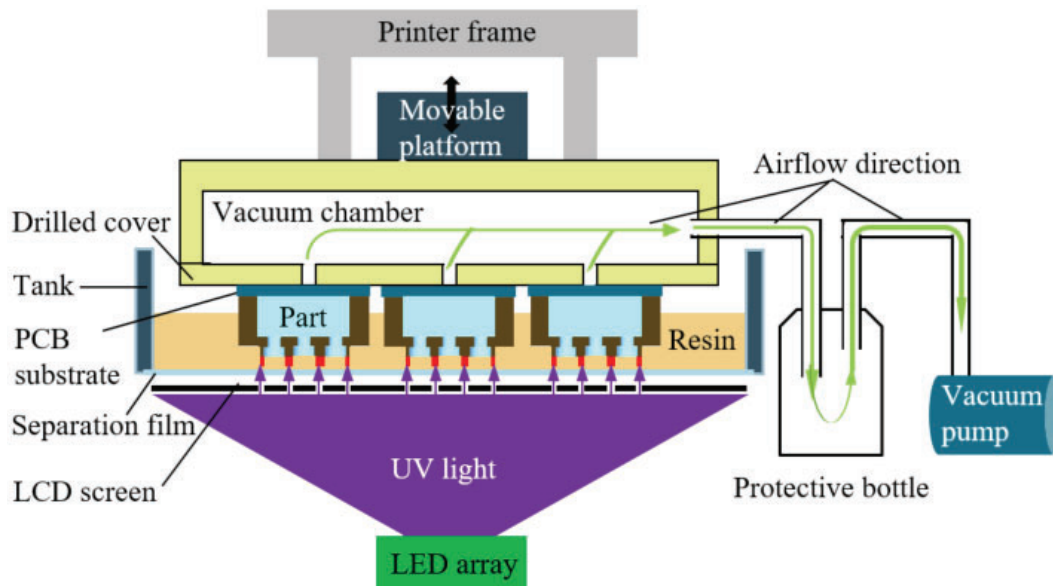


Fig. 2. The bottom-up LCD-based stereolithography machine with a vacuum suction system (includes the vacuum chamber, the protective bottle, and the pump)

Measurement methods

(1) Viscosity

The viscosity of the slurries was measured in the temperatures ranging from 20°C to 30°C using a Brookfield DV-II+Pro viscometer (Brookfield engineering laboratories, INC., USA). The process of selecting a spindle and speed for an unknown fluid usually is trial and error. The spindle type and speed combinations will produce satisfactory results when the applied torque is between 10 and 100% of the maximum permissible torque. Finally, the LV3-63# spindle and spinning rate of 20 rpm are selected in such a way that the torque values lie in this prescribed range.

(2) Microstructure

The resin/silica composite specimens were fractured and then sputter-coated with a gold layer (thickness 3nm). The fracture morphologies of the composite were examined by a PHILIPS scanning electron microscope (XL30 FEG) with an accelerating voltage of 10 kV.

(3) CTE

Thermo-mechanical analyzer (TMA) is the most common method used to measure the CTE of the resin related composites. This method measures the through-thickness expansion of the sample with temperature. Based on the standard ASTM E831, the dimensions of the samples for the CTE measurement were 8mm × 8mm × 10mm. The CTE below glass transition (α_1) and CTE above glass transition (α_2) were both measured using a Q400 TMA (T.A. Instruments, USA). The samples were heated from -40°C to 200°C at a constant rate of 5°C/min. The change in the sample thickness during heating was recorded with the change of temperature.

(4) Adhesion

To characterize adherence between microelectronic substrates and 3D printed part, the shear test and pull-off test was chosen (shown in Fig. 3 (a) and (b)). The contact area of the test samples can be calculated from the part size ($14 * 14 - 9 * 9 = 115 \text{ mm}^2$, shown in Fig. 3 (c)).

Four samples per adherence measurement were tested on the Instron 5567 machine. The same parameters and conditions (speed of testing: 2 mm/min, temperature: 20°C) were reproduced when tested the different samples.

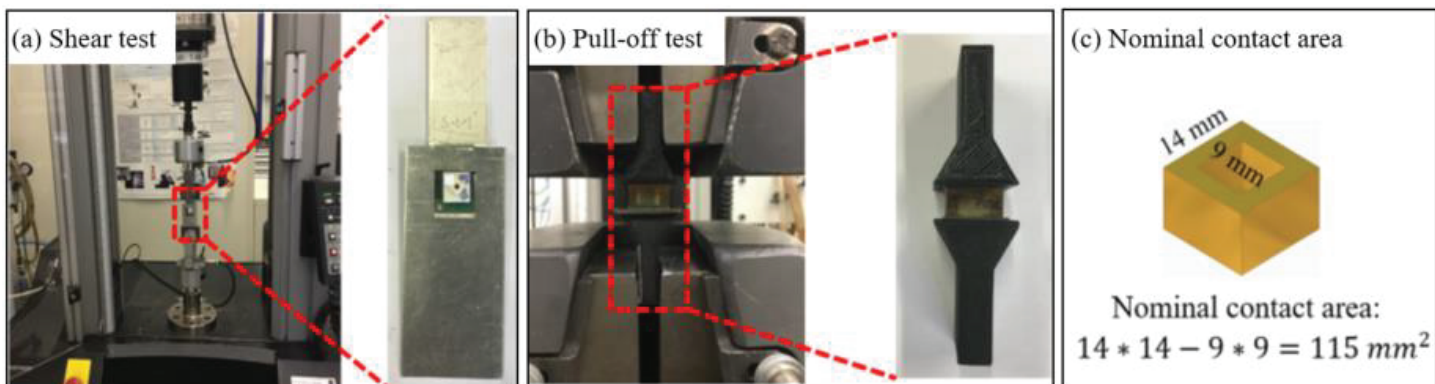


Fig. 3. The adhesion test. (a) Shear test device and setup, (b) Pull-off test device and setup, (c) Nominal contact area of the samples

(5) Thermal reliability

Specimens without visible defects were used for a thermal shock test only. The thermal shock test is performed utilizing a temperature shock chamber (tested in IMEC), the temperature in the shock chamber changes as shown in Fig.4. The specimens have been inspected visually and by pressure test (only 1 bar) after 100 cycles. Any leakage between the part/PCB or crack on the sample is regarded as a failure.

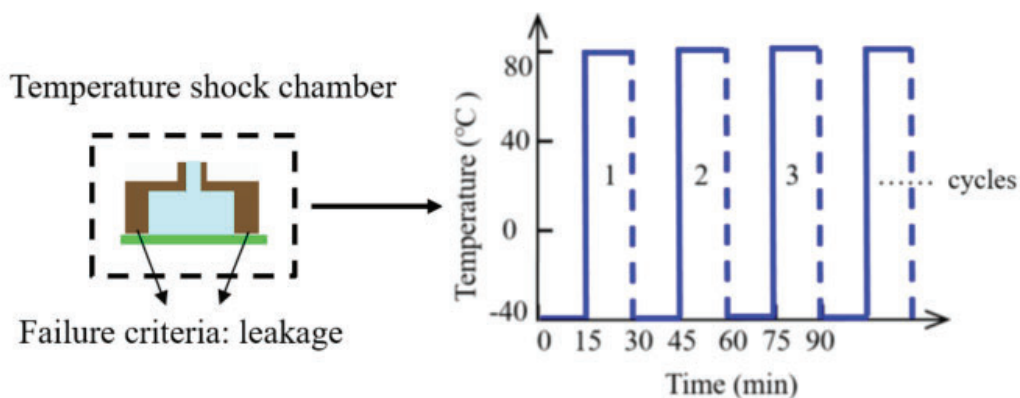


Fig. 4. The thermal shock test device and temperature change profile

Results and Discussion

Suspension viscosity and particle dispersion

The resin-powder suspensions for SLA applications have to satisfy the following requirements: the slurry should own good flowability to ensure satisfactorily recoating, the particles should be uniformly dispersed in the resin matrix to ensure the printing resolution and the quality of the printing parts. Some reports showed that the photoinitiator does not affect the suspension viscosity, but adding some dispersant could decrease the viscosity [29, 30]. After a series of experiments, based on the silica powder we used, the optimal concentration of dispersant is around 1.5 wt% to the powder. With this concentration of dispersant, the influence of the temperature on the viscosity of the suspensions containing 60 vol% of silica was studied.

The suspensions could work on our machine when the viscosity is less than 3000 mPa s (Brookfield DV-II+Pro viscometer, LV3-63# spindle, and 20 RPM), which means the suspensions can work well in the environment with temperature from 20°C to 30°C. The suspension viscosity decreases with the increasing of the temperature, e.g., the viscosity is reduced by nearly 800mPa s from 20°C to 30°C (shown in Fig. 5), which means the flowability of the suspension was improved as well. The temperature of the suspension will decrease during the printing process, especially for large parts that need a relatively long time, the temperature may drop from 30°C to 20°C or even lower. Therefore, we must ensure the suspension has a low viscosity and good flowability. A heating system and a mixer were used during the experiments.

The microstructures (shown in Fig. 6) also prove that the silica particles were uniformly dispersed in the resin matrix; this sample was fabricated at the temperature of ~25°C.

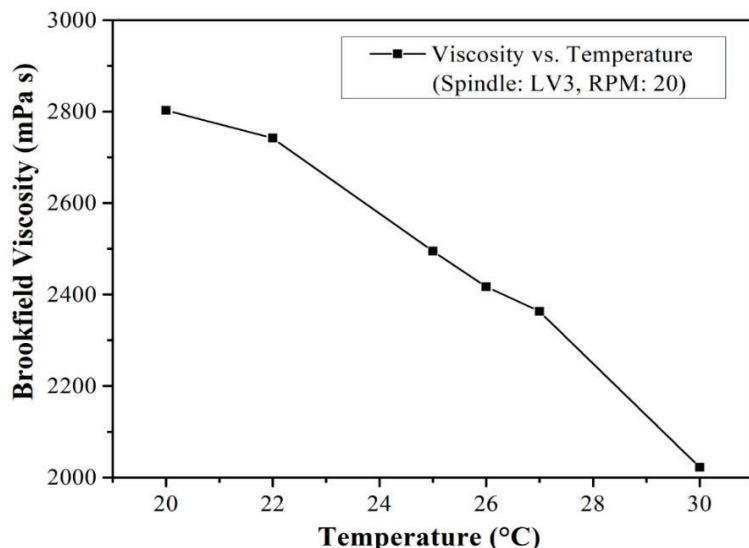


Fig. 5. Variation of the suspension viscosity with temperature (Silica: Resin=60 vol%: 40 vol%, 1.5 wt% dispersant)

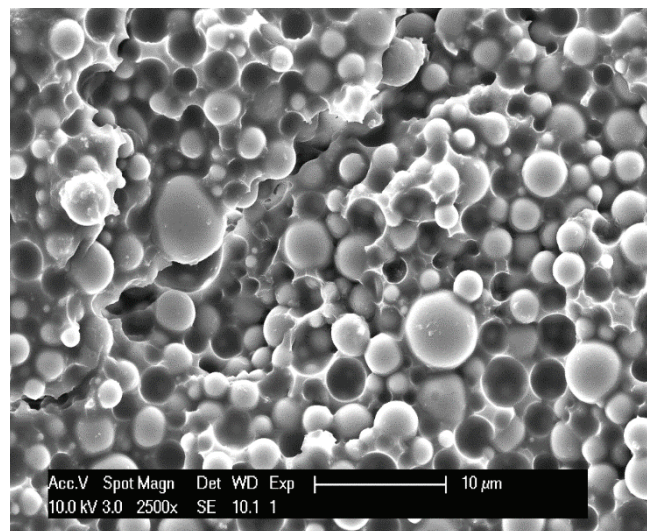


Fig. 6. The microstructure of resin-silica composite (printed at 25°C)

Thermal properties

As mentioned above, CTE is an essential parameter in semiconductor industry because a significant CTE mismatch between the fabrication parts and PCB substrate material can lead to the build-up of internal stresses during electronic device running and could lead to cracking of the interface. Therefore, if we want to print parts directly on the PCB, the CTE of the printing feedstock should be analyzed firstly. In this case, the linear CTE of the composites was analyzed. The linear CTE is defined as the ratio of the sample dimension change to the change in temperature per unit length (as the function shown in Fig. 7). From the curves in Fig. 7, the thermal expansion increases with the increase in temperature, and the CTEs were calculated from the slope. The change in the slope of the expansion curve indicates a transition of the material from one state to another (as a temperature range from 50°C to 90°C shown in Fig. 7). Therefore, α_1 (the CTE in the glassy state below the T_g) was taken from -40°C to 40°C and α_2 (the CTE above the T_g) was taken from 120°C to 200°C, the calculation results shown in Fig. 7.

The results show that the silica indeed works to reduce the composite CTE. Especially, α_1 is close to the CTE of commercial PCB, indicating the printed part can bond well on the PCB when the IC runs at a temperature below 90°C. Of course, this prediction should be proven by the below thermal cycling test.

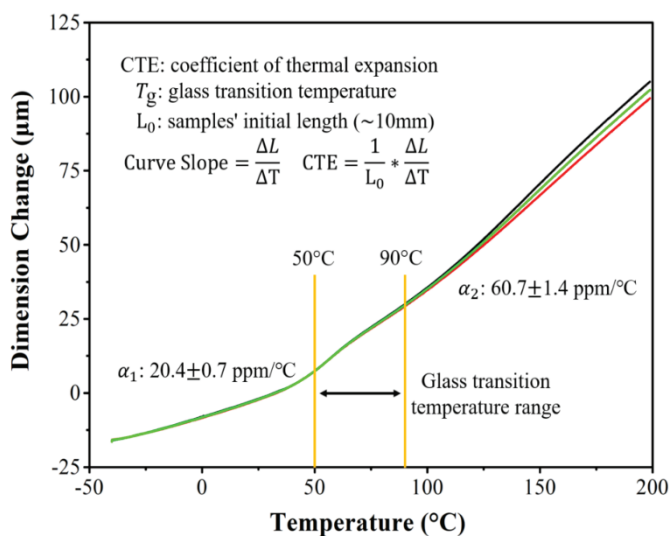


Fig. 7. Dimensional change with temperature of 3 samples (Manufactured under the same conditions with the SEM samples)

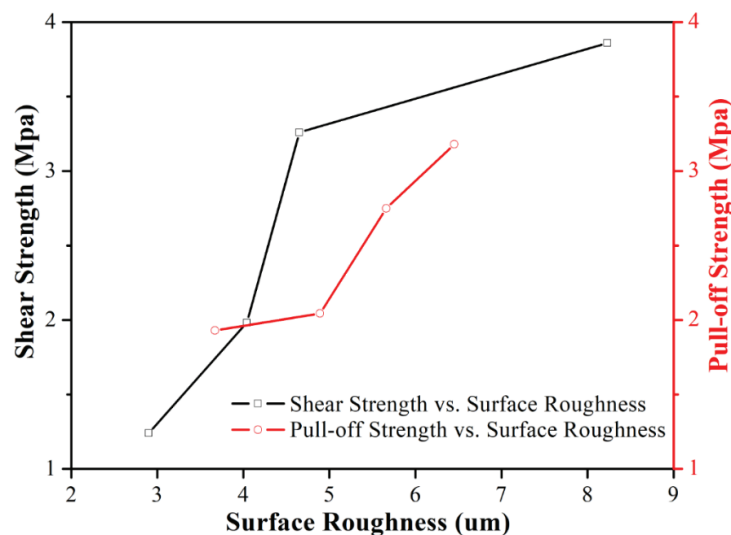


Fig. 8. The influence of surface roughness on adhesion forces
 Black line: shear test, red line: pull-off test

Adhesion properties

Commonly, the pull-off test (normal to the contact surface) and the shear test (parallel to the contact surface) were used to characterize the behavior of adhesion[10, 12, 31-34]. As we can see from Fig. 8, both the shear strength and the pull-off strength increased as the increase of the PCB surface roughness, which indicates that the adhesion on the part-PCB interface depends on their surface interactions. Based on the definition of surface roughness, the larger the roughness, the larger the actual contact area. It means that an uneven surface provides a higher interaction force than its smooth/flat counterpart.

Besides, we can also find that the rough surface has a greater effect on shear strength than pull-off strength. The microscale attachment mechanism for this type of adhesion is complex, which will be investigated in the future.

Thermal shock resistance

Ten samples were tested in the temperature shock chamber. After 100 cycles, only one sample failed during the test. It means 90% of the samples can survive after 100 cycles from -40°C to 80°C. This result indicates the prepared materials owned good CTE compatibility with the PCB substrate.

Conclusion

The Electronic-Mechanical Integrated Systems (EMIS) can be fabricated through AM-based hybrid manufacturing; this method is capable of fabricating protective/functional bodies for electronics. Visually, we find that this technology can manufacture the complex structure and cavity competently (no support needed).

Regarding the printing material, the silica-resin suspension containing 60 vol.% silica is uniformly enough to ensure the flowability during printing; at the same time, it has a low CTE which is close to that of the PCB material. The thermal cycling test indicated the prepared materials owned good CTE compatibility with the PCB substrate.

Adhesion properties between different part/PCB substrate showed the adhesion on the part-PCB interface depends on their surface interactions. The larger the interface roughness, the higher the interaction forces on the contact surface. The pull-off test indicated that the bonding force between the part-PCB is strong enough to keep them as an integrity system.

Apart from the above considerations, the print materials should be resistant to electrolyte corrosion, which will be further studied in the future.

Acknowledgments

Guanghai Fei warmly acknowledges the support provided by the China Scholarship Council (CSC) of the Ministry of Education, P. R. China. This work was supported by IMEC and the AM group of KU Leuven. Also, Guanghai Fei is grateful for support from Dr. Kehui Hu (Tsinghua University), Prof. Lei Nie (Xinyang normal university) for their experimental guidance. Furthermore, all the authors would like to acknowledge the support for the experimental tests done by Abdellah Salahouelhadj from IMEC (for the CTE measurement), Myriam Van de Peer from IMEC (for the thermal cycling measurement) and Danny Winant from MTM of KU Leuven (for the CTE measurement).

References

1. Lewis, J.A. and B.Y. Ahn, *Three-dimensional printed electronics*. Nature, 2015. **518**(7537): p. 42-43.
2. MacDonald, E. and R. Wicker, *Multiprocess 3D printing for increasing component functionality*. Science, 2016. **353**(6307): p. 8.
3. Olivas, R., R. Salas, D. Muse, E. MacDonald, and R.B. Wicker, *Structural electronics through additive manufacturing and micro-dispensing*. 2010, Proceedings from the IMAPS Symposium.
4. Cassie Gutierrez, Rudy Salas, Gustavo Hernandez, Dan Muse, Richard Olivas, Eric MacDonald, Michael D. Irwin, and Ryan Wicker, *CubeSat fabrication through additive manufacturing and micro-dispensing*. 2011, Proceedings from the IMAPS Symposium.

5. Lopes, A.J., E. MacDonald, and R.B. Wicker, *Integrating stereolithography and direct print technologies for 3D structural electronics fabrication*. Rapid Prototyping Journal, 2012. **18**(2): p. 129-143.
6. Espalin, D., D. W. Muse, E. MacDonald, and R. B. Wicker, *3D Printing multifunctionality: structures with electronics*. International Journal of Advanced Manufacturing Technology, 2014. **72**(5-8): p. 963-978.
7. Macdonald, E., R. Salas, D. Espalin, M. Perez, E. Aguilera, D. Muse, and R. B. Wicker, *3D Printing for the Rapid Prototyping of Structural Electronics*. Ieee Access, 2014. **2**: p. 234-242.
8. Li, J., T. Wasley, T. T. Nguyen, V. D. Ta, J. D. Shephard, J. Stringer, P. Smith, E. Esenturk, C. Connaughton, and R. Kay, *Hybrid additive manufacturing of 3D electronic systems*. Journal of Micromechanics and Microengineering, 2016. **26**(10): p. 14.
9. Wasley, T., J. Li, R. Kay, D. Ta, J. Shephard, J. Stringer, P. Smith, E. Esenturk, C. Connaughton, *Enabling Rapid Production and Mass Customisation of Electronics Using Digitally Driven Hybrid Additive Manufacturing Techniques*. in *66th IEEE Electronic Components and Technology Conference (ECTC)*. 2016, Las Vegas.
10. Aspar, G., B. Goubault, O. Lebaigue, J. C. Souriau, G. Simon, L. Di Cioccio, and Y. Brechet, *3D printing as a new packaging approach for MEMS and Electronic devices*. in *IEEE 67th Electronic Components and Technology Conference (ECTC)*. 2017, Lake Buena Vista.
11. Tiedje, T., S. Lungen, M. Schubert, M. Luniak, K. Nieweglowski, and K. Bock, *Will low-cost 3D Additive Manufactured Packaging replace the Fan-Out Wafer Level Packages?* in *IEEE 67th Electronic Components and Technology Conference (ECTC)*. 2017, Lake Buena Vista.
12. B., Goubault., Aspar. G., Souriau. J-C., Castagne. L., Simon. G., Di Cioccio. L., and Brechet. Y., *A new microsystem packaging approach Using 3D printing encapsulation process*. in *IEEE 68th Electronic Components and Technology Conference(ECTC)*. 2018, San Diego.
13. Lungen, S., T. Tiedje, K. Meier, K. Nieweglowski, K. Bock, *Reliability of 3D additive manufactured packages*. in *2018 7th Electronic System-Integration Technology Conference (ESTC)*. 2018, Dresden.
14. Li, J., Y. Wang, G. Z. Xiang, H. D. Liu, and J. L. He, *Hybrid Additive Manufacturing Method for Selective Plating of Freeform Circuitry on 3D Printed Plastic Structure*. Advanced Materials Technologies, 2019. **4**(2): p. 10.
15. Li, J., Y. X. Wang, E. K. Dong, and H. S. Chen, *USB-driven microfluidic chips on printed circuit boards*. Lab on a Chip, 2014. **14**(5): p. 860-864.
16. Dang, B., E. Colgan, F. H. Yang, M. Schultz, Y. Liu, Q. W. Chen, J. W. Nah, R. Polastre, M. Gaynes, G. McVicker, P. Parida, C. Tsang, J. Knickerbocker, and T. Chainer, *Integration and Packaging of Embedded Radial Micro-channels for 3D Chip Cooling*. in *66th IEEE Electronic Components and Technology Conference (ECTC)*. 2016, Las Vegas.
17. Wei, T.-W., H. Oprins, V. Cherman, I. De Wolf, E. Beynel, S. Yang, and M. Baelmans, *3D Printed Liquid Jet Impingement Cooler: Demonstration, Opportunities and Challenges*. in *IEEE 68th Electronic Components and Technology Conference (ECTC)*. 2018, San Diego.
18. Wei, Tiwei, Herman Oprins, Vladimir Cherman, Shoufeng Yang, Ingrid De Wolf, Eric Beyne, and Martine Baelmans, *Experimental characterization of a chip level 3D printed microjet liquid impingement cooler for high performance systems*. IEEE Transactions on Components, Packaging and Manufacturing Technology 2019. doi: 10.1109/TCPMT.2019.2905610 (Early Access).
19. Baikerikar, K.K. and A.B. Scranton, *Photopolymerizable liquid encapsulants for microelectronic devices*. Polymer, 2001. **42**(2): p. 431-441.
20. Mahrholz, T., J. Stangle, and M. Sinapius, *Quantitation of the reinforcement effect of silica nanoparticles in epoxy resins used in liquid composite moulding processes*. Composites Part A-Applied Science and Manufacturing, 2009. **40**(3): p. 235-243.
21. Suzuki, N., S. Kiba, and Y. Yamauchi, *Bimodal filler system consisting of mesoporous silica particles and silica nanoparticles toward efficient suppression of thermal expansion in silica/epoxy composites*. Journal of Materials Chemistry, 2011. **21**(38): p. 14941-14947.

22. Bae, C.J., D. Kim, and J.W. Halloran, *Mechanical and kinetic studies on the refractory fused silica of integrally cored ceramic mold fabricated by additive manufacturing*. Journal of the European Ceramic Society, 2019. **39**(2-3): p. 618-623.
23. Wong, C.P. and R.S. Bollampally, *Thermal conductivity, elastic modulus, and coefficient of thermal expansion of polymer composites filled with ceramic particles for electronic packaging*. Journal of Applied Polymer Science, 1999. **74**(14): p. 3396-3403.
24. Chen, Y.C., H.C. Lin, and Y.D. Lee, *The effects of filler content and size on the properties of PTFE/SiO₂ composites*. Journal of Polymer Research, 2003. **10**(4): p. 247-258.
25. Takenaka, K., *Negative thermal expansion materials: technological key for control of thermal expansion*. Science and Technology of Advanced Materials, 2012. **13**(1): p. 11.
26. Wicker, R.B. and E.W. MacDonald, *Multi-material, multi-technology stereolithography*. Virtual and Physical Prototyping, 2012. **7**(3): p. 181-194.
27. Vaezi, M., H. Seitz, and S.F. Yang, *A review on 3D micro-additive manufacturing technologies*. International Journal of Advanced Manufacturing Technology, 2013. **67**(5-8): p. 1721-1754.
28. Hamad, E. M., S. E. R. Bilatto, N. Y. Adly, D. S. Correa, B. Wolfrum, M. J. Schnoing, A. Offenhausser, and A. Yakushenko, *Inkjet printing of UV-curable adhesive and dielectric inks for microfluidic devices. Lab on a Chip*, 2016. **16**(1): p. 70-74.
29. Hinczewski, C., S. Corbel, and T. Chartier, *Ceramic suspensions suitable for stereolithography*. Journal of the European Ceramic Society, 1998. **18**(6): p. 583-590.
30. Wozniak, M., T. Graule, Y. de Hazan, D. Kata, and J. Lis, *Highly loaded UV curable nanosilica dispersions for rapid prototyping applications*. Journal of the European Ceramic Society, 2009. **29**(11): p. 2259-2265.
31. Lee, J., C. Majidi, B. Schubert, and R. S. Fearing, *Sliding-induced adhesion of stiff polymer microfibre arrays. I. Macroscale behaviour*. Journal of the Royal Society Interface, 2008. **5**(25): p. 835-844.
32. Schubert, B., J. Lee, C. Majidi, and R. S. Fearing, *Sliding-induced adhesion of stiff polymer microfibre arrays. II. Microscale behaviour*. Journal of the Royal Society Interface, 2008. **5**(25): p. 845-853.
33. Lucchetta, G., F. Marinello, and P.F. Bariani, *Aluminum sheet surface roughness correlation with adhesion in polymer metal hybrid overmolding*. Cirp Annals-Manufacturing Technology, 2011. **60**(1): p. 559-562.
34. Kim, S.L. and M.Y. Lyu, *Adhesive strengths between glass fiber-filled ABS and metal in insert molding with engraved and embossed metal surface treatments*. Polymer Engineering and Science, 2019. **59**: p. E93-E100.